LETTER

doi:10.1038/nature12423

Vesicular and non-vesicular transport feed distinct glycosylation pathways in the Golgi

Giovanni D'Angelo[1,2], Takefumi Uemura[3], Chia-Chen Chuang[4], Elena Polishchuk[1], Michele Santoro[1], Henna Ohvo-Rekilä[5], Takashi Sato[3], Giuseppe Di Tullio[6], Antonio Varriale[2], Sabato D'Auria[2], Tiziana Daniele[6], Fabrizio Capuani[1], Ludger Johannes[7,8], Peter Mattjus[5], Maria Monti[9], Piero Pucci[9], Roger L. Williams[10], John E. Burke[10], Frances M. Platt[4], Akihiro Harada[3,11] & Maria Antonietta De Matteis[1]

Newly synthesized proteins and lipids are transported across the Golgi complex via different mechanisms whose respective roles are not completely clear. We previously identified a non-vesicular intra-Golgi transport pathway for glucosylceramide (GlcCer)—the common precursor of the different series of glycosphingolipids—that is operated by the cytosolic GlcCer-transfer protein FAPP2 (also known as PLEKHA8) (ref. 1). However, the molecular determinants of the FAPP2-mediated transfer of GlcCer from the *cis*-Golgi to the *trans*-Golgi network, as well as the physiological relevance of maintaining two parallel transport pathways of GlcCer—vesicular and non-vesicular—through the Golgi, remain poorly defined. Here, using mouse and cell models, we clarify the molecular mechanisms underlying the intra-Golgi vectorial transfer of GlcCer by FAPP2 and show that GlcCer is channelled by vesicular and non-vesicular transport to two topologically distinct glycosylation tracks in the Golgi cisternae and the *trans*-Golgi network, respectively. Our results indicate that the transport modality across the Golgi complex is a key determinant for the glycosylation pattern of a cargo and establish a new paradigm for the branching of the glycosphingolipid synthetic pathway.

Complex glycosphingolipids (GSLs), which have key roles in cell signalling, adhesion, proliferation and differentiation[2], are synthesized in the Golgi complex from GlcCer, which is synthesized from ceramide at the cytosolic leaflet of early Golgi membranes[3,4]. Upon translocation to the luminal leaflet, GlcCer is galactosylated to lactosylceramide (LacCer), which can then be converted into complex GSLs in later Golgi compartments (Fig. 1a)[5]. GlcCer can be transported through the Golgi complex via membrane trafficking and via non-vesicular transfer owing to the action of the cytosolic GlcCer-transfer protein FAPP2, which fosters GSL synthesis[1,6]. However, the respective roles of the vesicular and non-vesicular transport of GlcCer remain to be defined[7].

We have addressed this question by assessing the consequences of *FAPP2* gene ablation in mice (Fig. 1b–d and Supplementary Fig. 1a). *FAPP2*$^{-/-}$ mice showed no overt phenotype. However, measurement of GSL levels in the kidneys, where FAPP2 is highly expressed (Fig. 1b and Supplementary Fig. 1b), highlighted a specific decrease in the globoside series of GSL, in particular in globotriaosylceramide (Gb3), in *FAPP2*$^{-/-}$ mice (Fig. 1e). Visualization of GSLs using the Shiga toxin B fragment (ShTxB) that binds Gb3 (ref. 8), the cholera toxin B fragment (ChTxB) that binds monosialotetrahexosylganglioside (GM1) (ref. 9), and anti-monosialodihexosylganglioside (GM3) antibodies confirmed the previously reported distribution of Gb3 in the mouse kidney[10,11] and showed a selective reduction of Gb3 staining in the *FAPP2*$^{-/-}$ kidneys (Fig. 1f, g) and in kidney tubular cells isolated from *FAPP2*$^{-/-}$ mice (Supplementary Fig. 2).

Thus, FAPP2, in line with its rather recent evolutionary appearance coincident with the divergence of multiple GSL branches[12], selectively controls one GSL branch *in vivo*. We then performed the analysis of GSL in cells knocked down for *FAPP2* by short interfering RNA (siRNA) treatment (Supplementary Fig. 3). As reported previously[1], *FAPP2* knockdown induced a 40% decrease in the levels of total GSLs (taken as the sum of LacCer, GM3 and Gb3) but, considering the individual GSL species, it lowered the levels of LacCer and Gb3 but not GM3 (Fig. 2a). In agreement with these biochemical measurements, a selective decrease in ShTxB staining was also observed in *FAPP2* knockdown cells (Supplementary Fig. 4a).

When we analysed the impact of *FAPP2* knockdown on newly synthesized GSLs in ^{3}H-sphingosine-labelled HeLa cells, we found that FAPP2 depletion inhibited the synthesis of ^{3}H-LacCer and ^{3}H-Gb3 at all time points (Fig. 2b and Supplementary Fig. 4b). *FAPP2* knockdown, however, also inhibited the synthesis of ^{3}H-GlcCer at early time points, in agreement with previous results[1], and as a consequence lowered the levels of ^{3}H-GM3 (Fig. 2b and Supplementary Fig. 4b). To circumvent changes in complex GSLs that might be secondary to the inhibition of GlcCer synthesis, we bypassed GlcCer synthesis by labelling the cells with fluorescent GlcCer (C12 BODIPY-GlcCer). Under these conditions, FAPP2 depletion selectively inhibited the synthesis of C12-BODIPY-Gb3 but not of C12-BODIPY-GM3 (Fig. 2c), indicating that the decrease in Gb3 but not in GM3 synthesis was a direct consequence of FAPP2 depletion. Systematic silencing of enzymes involved in GSL biosynthesis (Figs 1a, 2d and Supplementary Fig. 4c, d) highlighted that the GSL profile induced by FAPP2 silencing was similar to that induced by LacCer synthase (LCS) silencing in terms of a decrease in LacCer, but they differed in their effects on downstream GSL species: LCS knockdown induced a uniform decrease in Gb3 and GM3 whereas *FAPP2* knockdown selectively decreased Gb3. These results indicate that the GlcCer transported via FAPP2 feeds a pool of LacCer specifically destined to globoside (that is, Gb3) synthesis. Dynamic assessment of GSL metabolic fluxes followed by mathematical modelling corroborated this conclusion (Supplementary Fig. 5).

To search for the mechanisms responsible for the different sensitivities of Gb3 and GM3 synthesis to FAPP2 depletion, we studied the intra-Golgi distribution of Gb3 synthase (Gb3S) and of GM3 synthase (GM3S) by two independent approaches[7]. First, we measured the synthesis of Gb3 and GM3 in cells treated with brefeldin A (BFA), a toxin that redistributes the Golgi cisternae (but not the *trans*-Golgi network (TGN)) into the endoplasmic reticulum (ER) (generating an ER–Golgi intermixed compartment), interrupts vesicular trafficking from this intermixed compartment to the TGN[13], and releases FAPP2 from Golgi membranes[14]. BFA treatment decreased the synthesis of Gb3

[1]Telethon Institute of Genetics and Medicine, Via Pietro Castellino 111, 80131 Naples, Italy. [2]Institute of Protein Biochemistry National Research Council, Via Pietro Castellino 111, 80131 Naples, Italy. [3]Laboratory of Molecular Traffic, Department of Molecular and Cellular Biology, Institute for Molecular and Cellular Regulation, Gunma University, Gunma 371-8512, Japan. [4]Department of Pharmacology, University of Oxford, Mansfield Road, Oxford OX1 3QT, UK. [5]Department of Biosciences, Biochemistry, Åbo Akademi University, Artillerigatan 6 A III, BioCity, FI-20520 Turku, Finland. [6]Department of Cell Biology and Oncology, Consorzio Mario Negri Sud, Via Nazionale 8/A, 66030 Santa Maria Imbaro, Chieti, Italy. [7]Institut Curie Centre de Recherche, 26 rue d'Ulm, 75248 Paris Cedex 05, France. [8]CNRS, UMR144, F-75248 Paris, France. [9]Dipartimento di Scienze Chimiche and CEINGE Biotecnologie Avanzate, Università di Napoli Federicoll, ViaGaetano Salvatore 482, 80145 Napoli, Italy. [10]MRC Laboratory of Molecular Biology, Hills Road, Cambridge CB2 0QH, UK. [11]Department of Cell Biology, Osaka University, Osaka 565-0871, Japan.

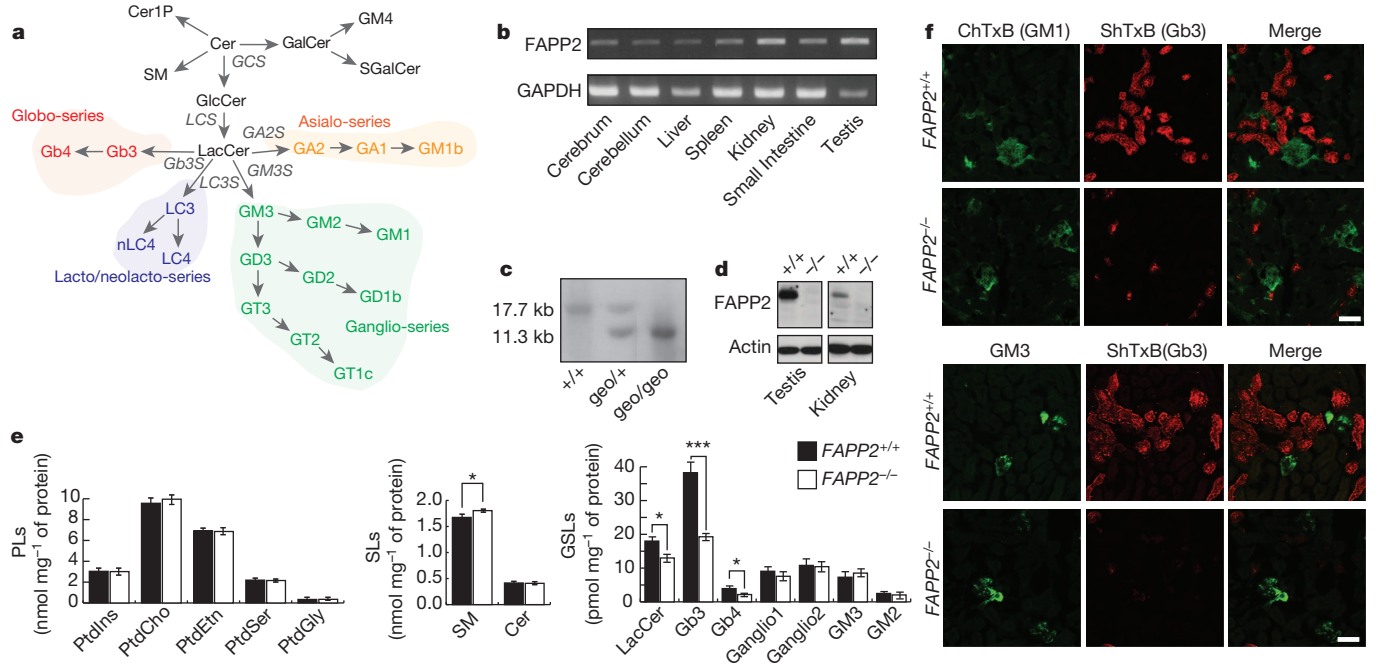

Figure 1 | FAPP2 selectively controls the levels of globosides *in vivo*. **a**, Simplified representation of the GSL synthetic pathway in vertebrates. GA2S, GA2 synthase; GCS, GlcCer synthase; LC3S, LC3 synthase. **b**, Expression of FAPP2 in mouse tissues. **c**, Southern blot of wild-type ($FAPP2^{+/+}$) and recombinant ($FAPP2^{geo/+}$ and $FAPP2^{geo/geo}$) mice tail DNA. See Supplementary Fig. 1b. **d**, FAPP2 levels in $FAPP2^{+/+}$ and $FAPP2^{-/-}$ testes and kidneys. **e**, Phospholipid (PL) and sphingolipid (SL) mass-spectrometry analysis, and GSL measurements of kidneys from $FAPP2^{+/+}$ ($n = 5$) and $FAPP2^{-/-}$ ($n = 10$) mice. Ganglio1, 2, unidentified gangliosides; Gb4, globoside; GM2, monosyalotrihexosylceramide; PtdCho, phosphatidylcholine; PtdIns, phosphatidylinositol; PtdEtn, phosphatidylethanolamine; PtdGly, phosphatidylglycine; PtdSer, phosphatidylserine; SM, sphingomyelin. Means ± s.e.m. **f**, ChTxB, ShTxB anti-GM3 staining of $FAPP2^{+/+}$ and $FAPP2^{-/-}$ kidney cortex sections. Representative pictures from at least five $FAPP2^{+/+}$ and five $FAPP2^{-/-}$ mice. Scale bars, 50 μm. $*P < 0.05$; $***P < 0.005$.

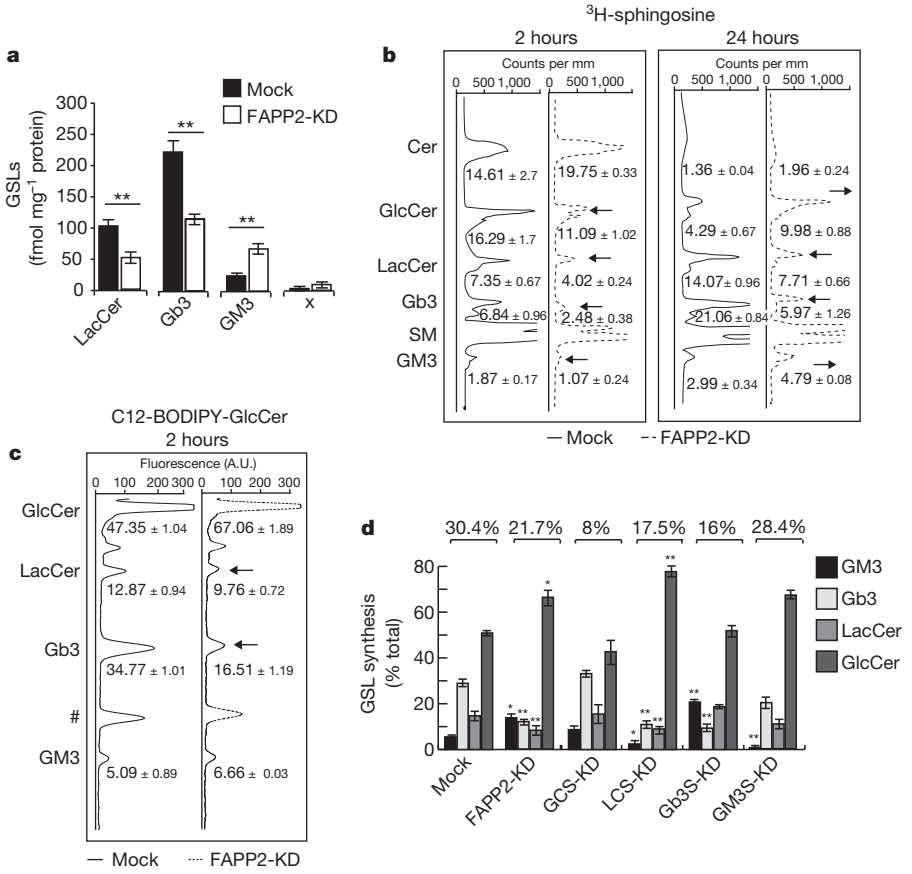

Figure 2 | FAPP2 is selectively required for Gb3 synthesis. **a**, GSL levels in HeLa cells. KD, knockdown; X, unassigned anionic GSL. **b**, High-performance thin-layer chromatography (HPTLC) profile of ^{3}H-sphingosine-labelled HeLa cells. Arrows denote changes induced by *FAPP2* knockdown. Numbers represent the percentage of each GSL species on total sphingolipids. **c**, HPTLC profile of C12-BODIPY-GlcCer-labelled HeLa cells. Arrows denote GSLs reduced by *FAPP2* knockdown; # represents unassigned peak and numbers represent the percentage of each GSL species on total GSL. A.U., arbitrary units. **d**, Effect of silencing of FAPP2 and of GSL synthetic enzymes on GSL species (expressed as percentage of total GSLs). Numbers represent the percentage of total GSLs on total sphingolipids. Means ± s.d. of at least three independent experiments. $*P < 0.05$; $**P < 0.01$.

but not that of GM3, indicating that the main fraction of endogenous Gb3S (but not of GM3S) resides in the TGN and thus remains segregated from its substrates that are synthesized in the BFA-induced intermixed ER–Golgi compartment (Fig. 3a). Second, we analysed the distribution of GM3S and Gb3S (Fig. 3b, c). In agreement with previous reports[6,15], we found that Gb3S is enriched in the TGN whereas GM3S is enriched in the Golgi cisternae. Moreover, consistent with its effect on GSL synthesis (Fig. 3a), BFA redistributed GM3S, but not Gb3S, to the ER (Supplementary Fig. 6).

The analysis of the role of FAPP2 was extended to other cell lines that also synthesize more complex gangliosides that, like GM3, were insensitive to FAPP2 depletion (Supplementary Fig. 7).

Thus, the synthesis of globosides at the TGN relies on the non-vesicular transport of GlcCer operated by FAPP2, whereas the synthesis of GM3 in the Golgi cisternae does not, eliciting the question as to whether GM3 synthesis depends instead on the vesicular transport of GlcCer. To address this question we inhibited intra-Golgi membrane trafficking[1] by treating cells with dicoumarol[1], by depleting the TRAPP component BET3 (also known as TRAPPC3) (ref. 1), or by depleting cytosolic phospholipase A_2 (cPLA$_2$) (ref. 16), and followed the transport of the temperature-sensitive mutant of vesicular stomatitis virus G protein (ts045-VSVG)[14]. As reported previously[1,16], these treatments suppressed the intra-Golgi progression of VSVG and strongly inhibited GM3 synthesis, but not Gb3 synthesis (Fig. 3d, e).

These results led us to propose that the vesicular transport of GlcCer feeds a pool of LacCer that is made in the Golgi cisternae and used for GM3 biosynthesis, whereas the non-vesicular transport of GlcCer via FAPP2 feeds a pool of LacCer that is made in the TGN and used in this compartment for globoside synthesis. This hypothesis generated some key predictions: (1) LCS should be present not only in the Golgi cisternae but also in the TGN; (2) other LacCer derivatives that, similarly to Gb3, are made at the TGN should depend on FAPP2; and (3) shifting the localization of GM3S from the Golgi cisternae to the TGN should make GM3 synthesis sensitive to FAPP2 depletion. We verified all of these predictions. First, LCS was found to localize both to the Golgi cisternae and to the TGN (Supplementary Fig. 8); second, *FAPP2* knockdown in SK-N-MC human neuronal cells selectively lowered the synthesis of gangliotriosylceramide (GA2), which is made in the TGN from LacCer (Fig. 1a and Supplementary Fig. 9a); third, GM3 synthesis, which is normally insensitive, becomes sensitive to FAPP2 depletion when a substantial fraction of GM3S is forced to localize at the TGN by expressing the enzyme at high levels (Supplementary Fig. 9b–d).

The selective requirement of FAPP2 for GSLs synthesized at the TGN, together with our previous observation that cells depleted of FAPP2 fail to concentrate GlcCer at the TGN[1], indicate that FAPP2 drives the transfer of GlcCer from the *cis*-Golgi—where GlcCer is synthesized—to the TGN, and raises the question of how this vectorial transport is sustained. We reasoned that in order to mediate the *cis*-Golgi-to-TGN transfer, apo-FAPP2 should be targeted to early Golgi membranes whereas GlcCer-bound FAPP2 should be targeted to the TGN. Thus, we compared the distribution of wild-type FAPP2 with that of a FAPP2 mutant, which is unable to bind GlcCer and thus is permanently apo (FAPP2(W407A))[1]. Although the main fraction of wild-type FAPP2 localizes at the TGN, the main fraction of FAPP2(W407A) localizes to the Golgi cisternae (Fig. 4a, b). Moreover, wild-type FAPP2 failed to localize at the TGN and was present mainly in the Golgi cisternae

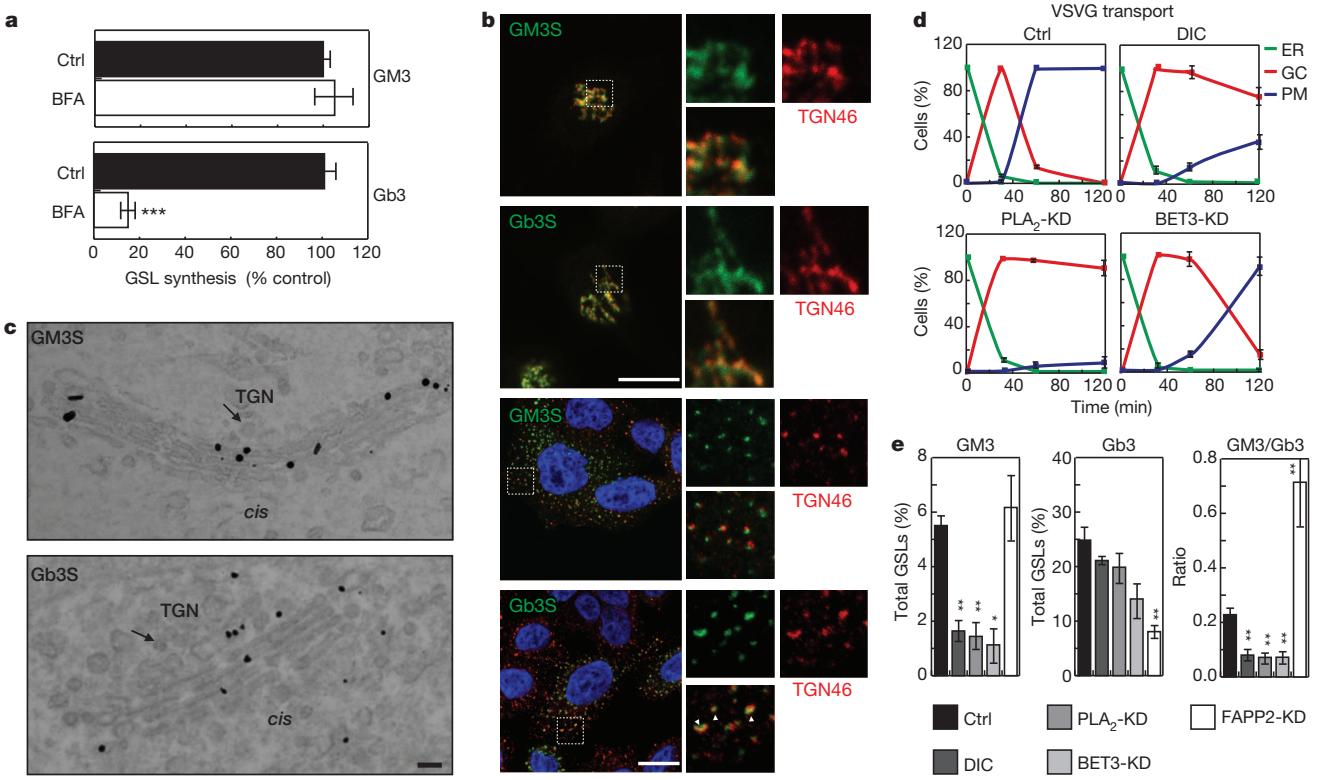

Figure 3 | Vesicular GlcCer transport feeds GM3 synthesis in the Golgi cisternae, whereas non-vesicular GlcCer transport feeds Gb3 synthesis in the TGN. **a**–**c**, Effect of BFA (5 μg ml^{-1}) on Gb3 and GM3 synthesis (**a**). Distribution of haemagglutinin (HA)–Gb3S and HA–GM3S evaluated by immunofluorescence (**b**) and by immunoelectron microscopy (**c**). In **b**, top panels represent untreated cells and bottom panels represent nocodazole-treated cells (3 h, 33 μM). Insets: enlargement of the boxed areas. The co-localization of HA–Gb3S and HA–GM3S with TGN46 was 50% and 14%, respectively. Data are representative of at least 30 cells per condition. Scale bar, 10 μm. **c**, Arrows represent clathrin-coated profiles at the TGN. Data are representative of at least 30 stacks. Scale bar, 100 nm. **d**, **e**, Effect of intra-Golgi trafficking blockage on VSVG transport (means ± s.d. in three independent experiments for at least 100 cells per time point) (**d**) and on GM3 and Gb3 synthesis (3-h ^{3}H-sphingosine pulse) (**e**). Means ± s.d. of three independent experiments. DIC, dicoumarol (200 μM); GC, Golgi complex; PM, plasma membrane. $*P < 0.05$; $**P < 0.01$; $***P < 0.005$.

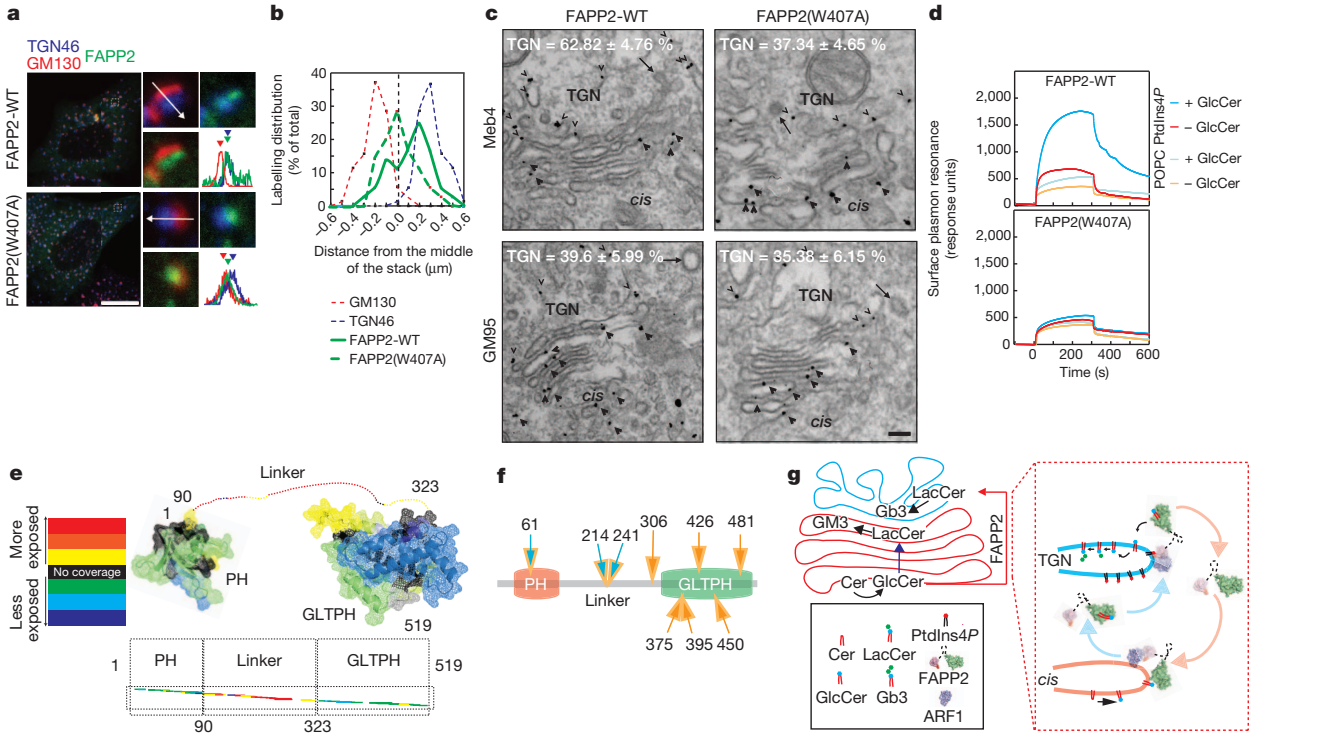

Figure 4 | GlcCer binding enhances the binding of FAPP2 to PtdIns4*P* and targets it to the TGN. **a**, Intra-Golgi distribution of wild-type FAPP2 (FAPP2-WT) and FAPP2(W407A) in nocodazole-treated cells (3 h, 33 μM). Right, enlargement of boxed areas and distribution of the maximal fluorescence intensity of FAPP2 along the *cis*-Golgi-to-TGN axis (white arrows). Scale bar, 10 μm. **b**, Quantification of the maximal labelling distribution of wild-type FAPP2 and FAPP2(W407A). The middle of the stack (0, black dashed line) is taken as a plane equidistant from GM130 and TGN46 fluorescence intensity peaks in 50 stacks per condition. **c**, Intra-Golgi distribution of wild-type FAPP2 and FAPP2(W407A) in Meb4 and GlcCer-deficient GM95 mouse cells. The percentage of TGN labelling is indicated. Means ± s.e.m. of at least 30 stacks per condition. Arrowheads represent Golgi cisternae staining, wedges represent TGN staining and arrows represent clathrin-coated profiles. Scale bar, 100 nm. **d**, Surface plasmon resonance analysis of the effect of GlcCer on FAPP2 binding to *1*-palmitoyl, *2*-oleoyl phosphatidylcholine (POPC)-PtdIns4*P* (98:2 mol:mol) liposomes. Results are representative of at least three independent experiments. PtdIns4*P* K_d value: 24 ± 0.9 μM for apo-FAPP2 and 6 ± 0.4 μM for GlcCer-bound FAPP2. **e**, Regions of FAPP2 showing different accessibility in HDX-MS were mapped on FAPP2. FAPP2 domains were modelled on the FAPP1 PH domain[18] and GLTPH domain[1,20]. **f**, Schematic representation of conformational changes induced by GlcCer loading on FAPP2 as assessed by HDX-MS (orange arrows) and controlled proteolysis-MS (blue arrows). Detailed results are presented in Supplementary Figs 12 and 13. **g**, Schematic representation of intra-Golgi non-vesicular (red arrow) and vesicular (blue arrow) transport of GlcCer. Inset: mechanism of FAPP2-mediated GlcCer-transfer directionality (cyan profiles, TGN; red profiles, Golgi cisternae; red arrows, targeting of apo-FAPP2 to the Golgi cisternae; cyan arrows, targeting of GlcCer-bound FAPP2 to the TGN.).

in cells that do not synthesize GlcCer[17], where FAPP2 is always apo (Fig. 4c). These results suggested that GlcCer binding positively regulates the targeting of FAPP2 to the TGN.

FAPP2 localization at the TGN is determined by its pleckstrin homology (PH) domain that coincidentally and independently[18] binds the small GTPase ARF1 and phosphatidylinositol 4-phosphate (PtdIns4*P*)[14], a phosphoinositide enriched at the TGN[19]. Single point mutations either in the PtdIns4*P*[14] or in the ARF-binding site[18] (Supplementary Fig. 10) abolish the recruitment of the PH domain to the Golgi complex (ref. 14 and data not shown), indicating a requirement for both binding sites. Interestingly, however, when these mutations are introduced into tandem forms of the FAPP PH-domain (di-PH), such that the di-PH has two binding sites either for ARF (di-PH-R18L) or for Ptdins4*P* (di-PH-E50A), the chimaeric proteins are able to localize to the Golgi complex, although with significantly different intra-Golgi distributions. In particular, a mutant FAPP-PH domain with a lower affinity for PtdIns4*P* and a higher affinity for ARF1 (di-PH-R18L) distributes throughout the Golgi stacks[14], whereas a mutant FAPP-PH domain with a lower affinity for ARF1 and a higher affinity for PtdIns4*P* (di-PH-E50A)[18] preferentially localizes to the TGN (Supplementary Fig. 10b), indicating that PtdIns4*P* dictates the TGN targeting of FAPP2.

We therefore assessed whether the preferential TGN association of GlcCer-bound FAPP2 could be due to the fact that it has a higher affinity for PtdIns4*P*. We found indeed that GlcCer loading (Supplementary information and Supplementary Fig. 11) increased FAPP2 binding to PtdIns4*P* (Fig. 4d), whereas it did not significantly affect the ability to bind ARF1 *in vitro* (not shown).

As FAPP2 binds GlcCer through its carboxy-terminal GLTP homology (GLTPH) domain[1,20] and PtdIns4*P* through its amino-terminal PH domain[14], the increase in PtdIns4*P* affinity induced by GlcCer binding suggested that GlcCer binding triggers a conformational change that is not limited to the GLTPH domain but is transmitted to more N-terminal regions. To gain insight into these conformational changes, we probed FAPP2 by hydrogen-deuterium exchange mass spectrometry (HDX-MS)[21]. The general profile of HDX-MS of FAPP2 indicated the presence of scarcely solvent-accessible N-terminal and C-terminal regions, corresponding to the PH-domain and the GLTPH domain, and the presence of a highly accessible and flexible intervening linker region (Fig. 4e). We then analysed the effects of GlcCer binding on the HDX-MS profile of FAPP2 and integrated this analysis with that of controlled proteolysis of FAPP2. The results of these analyses (Fig. 4f and Supplementary Figs 12 and 13) showed that the binding of GlcCer not only induced a stabilization of the GLTPH domain of FAPP2 but also affected the linker region interposed between the GLTPH domain and the PH domain, and on the PH domain itself, thus possibly having an impact on its PtdIns4*P* binding.

At this point a 'FAPP2 cycle' can be delineated (Fig. 4g): apo-FAPP2 associates with the *cis*-Golgi where it acquires GlcCer, resulting in a higher affinity of FAPP2 for PtdIns4*P*. FAPP2 then relocates to the PtdIns4*P*-enriched TGN where it delivers GlcCer.

Our findings establish a new paradigm for GSL biosynthesis whereby two branches receive their common precursor, GlcCer, from two parallel transport routes (Fig. 4g): the vesicular route feeds the LacCer pool used to make the ganglio-series in the Golgi cisternae, whereas the non-vesicular route mediated by FAPP2, which bypasses the intervening cisternae and delivers GlcCer to the TGN, feeds a TGN pool of LacCer converted *in loco* into GSLs of the globo- or asialo-series (Figs 1a and 4g). In a wider context, our results show how different modes of transporting a cargo through the Golgi complex channel the cargo itself towards distinct and otherwise potentially competing glycosylation pathways.

METHODS SUMMARY

FAPP2$^{-/-}$ mice were obtained following the procedure described in Supplementary Data and in ref. 22. High-performance liquid chromatography-based GSL measurements, metabolic labelling with ^{3}H-sphingosine, GSL extraction and HPTLC and analysis, as well as immunofluorescence and immunoelectron microscopy studies for subcellular protein localization assessments, were performed as described in ref. 1. Transport of ts045-VSVG was assessed as described previously[23]. Protein purification, fluorescence, circular dichroism and surface plasmon resonance studies were performed as described in refs 24, 25. HDX-MS was performed as in ref. 26. For statistical analysis, two-tailed Student *t*-tests were applied to the data. $*P < 0.05$; $**P < 0.01$; $***P < 0.005$.

Full Methods and any associated references are available in the online version of the paper.

Received 21 June 2012; accepted 25 June 2013.
Published online 4 August 2013.

1. D'Angelo, G. *et al.* Glycosphingolipid synthesis requires FAPP2 transfer of glucosylceramide. *Nature* **449,** 62–67 (2007).
2. Hakomori, S. I. Structure and function of glycosphingolipids and sphingolipids: recollections and future trends. *Biochim. Biophys. Acta* **1780,** 325–346 (2008).
3. Jeckel, D., Karrenbauer, A., Burger, K. N., van Meer, G. & Wieland, F. Glucosylceramide is synthesized at the cytosolic surface of various Golgi subfractions. *J. Cell Biol.* **117,** 259–267 (1992).
4. Futerman, A. H. & Pagano, R. E. Determination of the intracellular sites and topology of glucosylceramide synthesis in rat liver. *Biochem. J.* **280,** 295–302 (1991).
5. Hannun, Y. A. & Obeid, L. M. Principles of bioactive lipid signalling: lessons from sphingolipids. *Nature Rev. Mol. Cell Biol.* **9,** 139–150 (2008).
6. Halter, D. *et al.* Pre- and post-Golgi translocation of glucosylceramide in glycosphingolipid synthesis. *J. Cell Biol.* **179,** 101–115 (2007).
7. Maccioni, H. J., Quiroga, R. & Ferrari, M. L. Cellular and molecular biology of glycosphingolipid glycosylation. *J. Neurochem.* **117,** 589–602 (2011).
8. Jacewicz, M., Clausen, H., Nudelman, E., Donohue-Rolfe, A. & Keusch, G. T. Pathogenesis of shigella diarrhea. XI. Isolation of a shigella toxin-binding glycolipid from rabbit jejunum and HeLa cells and its identification as globotriaosylceramide. *J. Exp. Med.* **163,** 1391–1404 (1986).
9. van Heyningen, S. V. Cholera toxin: interaction of subunits with ganglioside G_{M1}. *Science* **183,** 656–657 (1974).
10. Psotka, M. A. *et al.* Shiga toxin 2 targets the murine renal collecting duct epithelium. *Infect. Immun.* **77,** 959–969 (2009).
11. Okuda, T. *et al.* Targeted disruption of Gb3/CD77 synthase gene resulted in the complete deletion of globo-series glycosphingolipids and loss of sensitivity to verotoxins. *J. Biol. Chem.* **281,** 10230–10235 (2006).
12. D'Angelo, G., Vicinanza, M. & De Matteis, M. A. Lipid-transfer proteins in biosynthetic pathways. *Curr. Opin. Cell Biol.* **20,** 360–370 (2008).
13. Chege, N. W. & Pfeffer, S. R. Compartmentation of the Golgi complex: brefeldin-A distinguishes trans-Golgi cisternae from the trans-Golgi network. *J. Cell Biol.* **111,** 893–899 (1990).
14. Godi, A. *et al.* FAPPs control Golgi-to-cell-surface membrane traffic by binding to ARF and PtdIns(4)P. *Nature Cell Biol.* **6,** 393–404 (2004).
15. Yamaji, T., Nishikawa, K. & Hanada, K. Transmembrane BAX inhibitor motif containing (TMBIM) family proteins perturbs a *trans*-Golgi network enzyme, Gb3 synthase, and reduces Gb3 biosynthesis. *J. Biol. Chem.* **285,** 35505–35518 (2010).
16. San Pietro, E. *et al.* Group IV phospholipase $A_2\alpha$ controls the formation of inter-cisternal continuities involved in intra-Golgi transport. *PLoS Biol.* **7,** e1000194 (2009).
17. Ichikawa, S., Nakajo, N., Sakiyama, H. & Hirabayashi, Y. A mouse B16 melanoma mutant deficient in glycolipids. *Proc. Natl Acad. Sci. USA* **91,** 2703–2707 (1994).
18. He, J. *et al.* Molecular basis of phosphatidylinositol 4-phosphate and ARF1 GTPase recognition by the FAPP1 pleckstrin homology (PH) domain. *J. Biol. Chem.* **286,** 18650–18657 (2011).
19. D'Angelo, G., Vicinanza, M., Di Campli, A. & De Matteis, M. A. The multiple roles of PtdIns(4)*P*–not just the precursor of PtdIns(4,5)*P*2. *J. Cell Sci.* **121,** 1955–1963 (2008).
20. Kamlekar, R. K. *et al.* The glycolipid transfer protein (GLTP) domain of phosphoinositol 4-phosphate adaptor protein-2 (FAPP2): structure drives preference for simple neutral glycosphingolipids. *Biochim. Biophys. Acta* **1831,** 417–427 (2013).
21. Yan, X., Watson, J., Ho, P. S. & Deinzer, M. L. Mass spectrometric approaches using electrospray ionization charge states and hydrogen-deuterium exchange for determining protein structures and their conformational changes. *Mol. Cell. Proteomics* **3,** 10–23 (2004).
22. Sato, T. *et al.* The Rab8 GTPase regulates apical protein localization in intestinal cells. *Nature* **448,** 366–369 (2007).
23. D'Angelo, G. *et al.* GRASP65 and GRASP55 sequentially promote the transport of C-terminal valine-bearing cargos to and through the Golgi complex. *J. Biol. Chem.* **284,** 34849–34860 (2009).
24. Zhai, X. *et al.* Glycolipid acquisition by human glycolipid transfer protein dramatically alters intrinsic tryptophan fluorescence: insights into glycolipid binding affinity. *J. Biol. Chem.* **284,** 13620–13628 (2009).
25. Ohvo-Rekilä, H. & Mattjus, P. Monitoring glycolipid transfer protein activity and membrane interaction with the surface plasmon resonance technique. *Biochim. Biophys. Acta* **1808,** 47–54 (2011).
26. Burke, J. E., Perisic, O., Masson, G. R., Vadas, O. & Williams, R. L. Oncogenic mutations mimic and enhance dynamic events in the natural activation of phosphoinositide 3-kinase p110alpha (*PIK3CA*). *Proc. Natl Acad. Sci. USA* **109,** 15259–15264 (2012).

Supplementary Information is available in the online version of the paper.

Acknowledgements We thank A. Luini, C. Wilson and D. Priestman for discussions, A. Egorova for help with electron microscopy, G. Liebisch, A. Sigruener and G. Schmitz for lipidomic analysis. M.A.D.M. acknowledges the support of Telethon (GSP08002 and GGP06166), Associazione Italiana per la Ricerca sul Cancro (AIRC) (IG 8623), and the EU (FP7 Lipidomicnet). G.D.'A. acknowledges the support of AIRC (MFAG 10585). P.M. acknowledges the support of Academy of Finland and Sigrid Jusélius Foundation. C.-C.C. was funded by a Study Abroad Scholarship from the Taiwan Ministry of Education.

Author Contributions M.A.D.M. supervised the entire project; M.A.D.M. and G.D.'A. wrote the manuscript with comments from all co-authors; G.D.'A., with the help of M.S., designed and conducted at TIGEM the experiments of sphingolipid labelling, membrane trafficking, immuno-localization and controlled proteolysis. M.S. designed the strategy and produced plasmid vectors. M.S. and G.D.T. prepared recombinant proteins, anti-FAPP2 and anti-BET3 antibodies. T.U. and T.S. generated and characterized *FAPP2*$^{geo/geo}$ and *FAPP2*$^{-/-}$ mice under the supervision of A.H. C.-C.C. conducted the HPLC measurements of GSLs under the supervision of F.M.P. L.J. provided the Cy3-ShTxB. E.P. and T.D. conducted the electron microscopy experiments. H.O.-R. conducted the surface plasmon resonance experiments under the supervision of P.M. A.V. conducted the tryptophan fluorescence and circular dichroism experiments under the supervision of S.D'.A. F.C. and G.D'.A. produced the mathematical model for GSL metabolism. M.M. and P.P. performed and interpreted the MS analysis; R.L.W. and J.E.B. performed and interpreted the HDX analysis.

Author Information Reprints and permissions information is available at www.nature.com/reprints. The authors declare no competing financial interests. Readers are welcome to comment on the online version of the paper. Correspondence and requests for materials should be addressed to M.A.D.M. (dematteis@tigem.it).

METHODS

Reagents and antibodies. All chemical reagents were of analytical grade or higher and purchased from Sigma unless otherwise specified. Cell culture media were from Invitrogen. Polyclonal antibodies against human FAPP2, BET3, cPLA$_2$IVa and GM130 were raised in rabbits using glutathione *S*-transferase fusion proteins as immunogens. All were affinity purified on their corresponding immunogens. The anti-VSVG clone P5D4, anti-Flag M2 and anti-HA monoclonal antibodies, and the anti-rabbit and anti-mouse IgG Cy3-conjugated antibodies were from Sigma. The Alexa 488-conjugated ChTxB fragment was from Invitrogen. The Cy3-conjugated ShTxB fragment was prepared as described[27]. The mouse monoclonal antibody against GM3 (clone 2590) was from Cosmo Bio Co. Sheep polyclonal antibodies against TGN46 were from AbD Serotech. The Alexa 488 goat anti-mouse and anti-rabbit IgG antibodies were from Molecular Probes. All unlabelled purified lipids were from Avanti Polar Lipids. ^{3}H-sphingosine was from PerkinElmer. Stock solutions of GSLs were prepared in chloroform/methanol (2:1 by volume) and of other lipids in hexane/2-propanol (3:2 by volume). Lipid solutions were stored in the dark at −20 °C and warmed to room temperature before use.

FAPP2 Knockout mice. Mice were from the C57BL/6 strain. All animal procedures were performed in accordance with the guidelines of the Animal Care and Experimentation Committee of Gunma University, and all animals were bred in the Institute of Animal Experience Research of Gunma University. *FAPP2* knockout mice were generated following the procedure described in Supplementary information. Histological, immunofluorescence microscopy and X-gal staining were performed as previously described[22,28,29].

Cell culture. HeLa, Meb4, GM95, HepG2, HK2, COS7 and MDCK cells were grown and transiently transfected by TransIT-LT1 (Mirus Bio) as described in ref. 1. Stably-expressing HeLa-GM3S cells were obtained after transfection of the 3×HA–GM3S coding plasmid and selection in the presence of G418 (Invitrogen) and screening of monoclonal colonies by indirect immunofluorescence.

Plasmids and constructs. Most of the constructs used in this study were obtained from HeLa RNA by RT–PCR and cloning into appropriate vectors. In brief, total RNA was isolated from HeLa cells; RT–PCR was performed using a poly dT oligo as a primer. The complementary DNA obtained was used as a template for PCR, using the following primers: for Gb3S: forward 5′-GTTGAATTCGATCTGG GGATACCATGTCC-3′, reverse 5′-CACCTCGAGCAAGTACATTTTCATGG CCTC-3′; for GM3S: forward 5′-CAGGAATTCAGAATGAGAAGGCCCA GCTTGTTA-3′, reverse 5′-AACGCGGCCGCTGAAATTCACGATCAATGC CTCCA-3′; for LCS: forward 5′-ATAGAATTCTGGCTGCAGCATGCGCGC-3′, reverse 5′-CGCGATATCAAGTACTCGTTCACCTGAGCCA-3′. The PCR products were cloned into a linearized pCR2.1 vector, and processed for automatic sequencing. All of the cloned sequences matched the sequence reported in databases for human Gb3S (AF513325), GM3S (AY152815.2) and LCS (B4GALT5; (NM_004776)). The DNAs corresponding to the various coding sequences were then subcloned into EcoRI/XhoI (Gb3S), EcoRI/NotI (GM3S), EcoRI/EcoRV sites of pCDNA3-3XHA at C-terminus or p3XFLAG-CMV-14.

Green fluorescent protein (GFP)–FAPP2 wild-type and W407A constructs were obtained as described in ref. 1; recombinant GST–FAPP2 wild-type, GST–FAPP2(W407A), His-FAPP2 wild type and His-FAPP2(W407A) were produced in *Escherichia coli* as described in ref. 1.

GFP–diFAPP2PH-wild type and E50A were obtained as follows: GFP–FAPP2 wild-type DNA was used as a template for two distinct PCR reactions using as primers: PCR (a): 5′-TCTGAATTCATGGAGGGGGTGCTGTACA-3, 5′-TAT GGTACCGAGCAAGCAAGCCTTGGCTGATCCC-3; PCR (b): 5′-TATGGT ACCTTGCTGGAGGGGGTGCTGTACAAGTG-3, 5′-TCACTCGAGTTAGCA AGCCTTGGCTGATCC-3. Products from PCR (a) were subcloned into EcoRI/KpnI sites of vector pEGFP-C1 to obtain construct pEGFP-FAPP2PH. Subsequently, products from PCR (b) were subcloned into KpnI/XhoI sites of the pEGFP-FAPP2PH construct to obtain GFP–diFAPP2PH-wild type. A similar procedure was applied to obtain the GFP–diFAPP2PH(E50A) mutant using as a template GFP–FAPP2(E50A) DNA. GFP–FAPP2(E50A) was obtained from wild-type GFP–FAPP2 by site-directed mutagenesis using the primers 5′-GAGCATACAAATGGCAGTCTGTGCAATTCAAGTTCATTCTGTAG-3′ and 5′-CTACAGAATGAACTTGAATTGCACAGACTGCCATTTGTATGCTC-3′.

siRNA treatments. The siRNAs for human FAPP2 (NM_001197026), GCS (NM_003358), BET3 (NM_014408), B4GALT5 (NM_004776), B4GALT6 (NM_004775), SIAT9/GM3S (AY152815.2), A4GALT/Gb3S (NM_017436), PLA$_2$ (NM_001199562) comprised mixtures of at least three siRNA duplexes (Supplementary Table 1) and were obtained from Dharmacon. HeLa, HK2, HepG2 and MDCK cells were plated at 30% confluence in 12-well plates and transfected with 120–150 pmol of siRNAs with Oligofectamine (Invitrogen) or Dharmafect4 (Dharmacon), in accordance with the manufacturer's protocol. At 72 h after the initial treatment with siRNA, the cells were processed directly. Silencing efficiency was evaluated either by western blot (Supplementary Fig. 2) or by quantitative PCR (Supplementary Fig. 4b) using specific primers (Supplementary Table 1).

Measurement of GSLs. Metabolic labelling with ^{3}H-sphingosine or ^{14}C-galactose, GSL extraction and HPTLC and analysis were performed as described in refs 1, 6.

Immunofluorescence and morphometric analysis. All immunofluorescence experiments were performed as described previously[1,14]. Images are confocal optical slices obtained using an LSM 710 (Zeiss) confocal microscope. Co-localization analysis was performed as described in ref. 14 or by using an object-based co-localization method included in the JACoP v2.0 application for ImageJ[30]. In brief, individual mini-stacks in nocodazole-treated cells were considered as objects whose mass-centre position was calculated after segmentation. The perfect coincidence of mass-centre positions for two distinct labellings (that is, Gb3S/TGN46 or GM3S/TGN46) in a single mini-stack was considered as a positive co-localization event.

Immunoelectron microscopy. Immunoelectron microscopy was performed in transfected HeLa, Meb4 and GM95 cells as described previously[1].

VSVG intracellular transport assay. Transport of ts045-VSVG was assessed as described previously[23].

Statistical analysis. For statistical analysis, two-tailed Student *t*-tests were applied to the data. $*P < 0.05$; $**P < 0.01$; $***P < 0.005$.

27. Mallard, F. & Johannes, L. Shiga toxin B-subunit as a tool to study retrograde transport. *Methods Mol. Med.* **73,** 209–220 (2003).
28. Muramatsu, K. *et al.* Neuron-specific recombination by Cre recombinase inserted into the murine *tau* locus. *Biochem. Biophys. Res. Commun.* **370,** 419–423 (2008).
29. Hashimoto, Y. *et al.* Neuron-specific and inducible recombination by Cre recombinase in the mouse. *Neuroreport* **19,** 621–624 (2008).
30. Bolte, S. & Cordelieres, F. P. A guided tour into subcellular colocalization analysis in light microscopy. *J. Microsc.* **224,** 213–232 (2006).